PROBLEM 6: Neural Decoding and Modulation in Patients with Tetraplegia

Charles Kristopher Garrett[1], Matthew Labrum[2], Martial Longla[3],
Guy-vanie Marcias Miakonkana[4], Varada Sarovar[5], Guolin Zhao[6]

Problem Presenter:
Chad Bouton
Battelle Memorial Institute

Abstract

This work was part of a pilot clinical study, the first of its kind, involving the implantation of a 96 electrode array in the human brain for up to a full year. The work described here involved two of the subjects in the study, one of which was a stroke victim (or "SCI3"), and the other had Amyotrophic Lateral Sclerosis (or "ALS"). Both subjects were tetraplegic and also unable to speak. The intent of this study was to determine if intended movements would evoke neural activity that could be successfully decoded and allow the subjects to control various devices in their environment and communicate through a personal computer. Neural decoding algorithms were developed to interpret the intracortical activity in the primary motor cortex of both subjects. The previous work employed a support vector machine method to classify different arm movements. In this current work, we modify the existing algorithm to improve the models. We also developed heat maps to spatially identify the neuronal activities associated with various imagined movements.

1 Introduction

BrainGate^{TM}, a Brain-Computer Interface (BCI) system founded by *Cyberkinetics*, was developed to enable severely motor-impaired individuals to communicate, interact and function through their thoughts. The goal is to allow them to communicate, use their PCs, and even control a wheelchair by decoding their thoughts with the electrode array implanted in the Primary Motor Cortex (M1).

With the aim of isolating and predicting arm movements, *Battelle* developed user training methods and neural decoding algorithms to process signals from the electrode array with 96 channels. In the pilot clinical study, two patients volunteered to participate. One was a 54 year old female stroke victim (or "SCI3") and the other was a 36 year old male, diagnosed with Amyotrophic Lateral Sclerosis (or "ALS"). Both of them were tetraplegic and unable to speak. In the study, an intended motion survey was conducted to look at neural modulation (changes in neuronal firing patterns) for several visually cued movements paired as:

- Shoulder Flexion and Extension
- Shoulder Abduction and Adduction
- Elbow Flexion and Extension
- Wrist Flexion and Hyperextension
- Wrist Radial and Ulnar Deviation
- Wrist Pronation and Supination
- Hand Open and Close

[1]University of Texas at Arlington
[2]Washington State University
[3]Univeristy of Cincinnati
[4]Auburn Univeristy
[5]California State University at East Bay
[6]North Carolina State University

The algorithms developed during the study were successful in allowing the patient to control a motorized wheelchair through those imagined movements. In this project, we modified some of the existing algorithms to improve the detection of different movements. The adapted model presents more robustness with the data collected during the four-month period. Higher detection rates are given by using the proposed model compared to the existing model, while maintaining the false positives at a similar level. In addition, heat maps which describe the spatial distribution of active neurons during various motions are plotted. These maps are employed to analyze the evolution of neuronal firing patterns over time and to identify the neurons corresponding to the various movements.

1.1 Data description

The implant consisted of 96 electrodes arranged in a 10×10 array, with the corners left unused. Each electrode detects electrical activity from neurons close to it and records that activity over time; this recording constitutes the data.

Each data set is referred to as a task and is composed of the neural activity recorded as the subject is given cues alternating between "rest" and some movement (e.g., "shoulder up"). Furthermore, a task consisted of a training period and sometimes a test period. The data collected in the training period were used to develop classifiers and the data from the test period were used to evaluate the performance of the classifiers. Finally, a collection of tasks in a day is a session, and the entire data set for each subject consists of multiple sessions.

For algorithm development we employed MATLAB 7.9.0 (R2009b), and we used SAS® software, Version 9.2, for statistical analysis of the results.

2 Support vector machine (SVM)

The brain's electromagnetic (EM) field reflects a representation of the information in the neurons [1]. We believed that the firing rates of the neurons change for each intended movement. Thus, methods developed in data classification were applied to discriminate between neuron firing rates. Support vector machine (SVM) is such an approach to assign points into one of two disjoint classes (or half-spaces), which we refer to as a classifier. In this section, we first briefly introduce the existing model in Section 2.1, and the proposed model is discussed in Section 2.2.

2.1 Proximal support vector machine (PSVM)

The standard SVM requires linear programming or solving a quadratic which may involve complex computation and large amounts of memory. Proximal support vector machines were then introduced to simplify the calculations. The PSVM classifies points depending on proximity to one of two parallel planes that are pushed as far apart as possible [2].

Suppose m time points are separated into two classes, denoted by $A+$ and $A-$, in the n-dimensional real space $\mathbb{R}^n$. Let A be the $m \times n$ matrix corresponding to these time points, and D be the $n \times n$ diagonal matrix with $+1$ or -1, where $+1$ and -1 correspond to $A+$ and $A-$, respectively. The Proximal support vector machine with a linear kernel is then given by the following optimization problem with parameter $\nu > 0$.

$$\min_{(w,\gamma,y)\in\mathbb{R}^{n+m+1}} f(w,\gamma,y) = \min_{(w,\gamma,y)\in\mathbb{R}^{n+m+1}} \left[\frac{\nu}{2}\|y\|^2 + \frac{1}{2}(w^T w) + \frac{1}{2}\gamma^2\right], \tag{1}$$

$$\text{s.t } D(Aw - e\gamma) + y = e,$$

where e is the vector of ones.

2.1.1 Standard method

The planes $x^T w - \gamma = \pm 1$ produced by the PSVM are not bounding planes, but can be thought of as "proximal" planes, around which the points of each class are clustered [2].

The solution for this constrained problem is obtained using the Lagrangian:

$$L(w,\gamma,y,u) = \frac{\nu}{2}\|y\|^2 + \frac{1}{2}(w^T w) + \frac{1}{2}\gamma^2 - u^T(D(Aw - e\gamma) + y - e). \tag{2}$$

Here, $u \in \mathbb{R}^m$ is the Lagrange multiplier associated with the constraint in Equation (1). Thus, we have the optimality conditions:

$$\begin{aligned} w - A^T Du &= \mathbf{0}, \\ \gamma + e^T Du &= \mathbf{0}, \\ \nu y - u &= \mathbf{0}, \\ D(Aw - e\gamma) + y - e &= \mathbf{0}. \end{aligned}$$

By solving the equations, we have $w = A^T Du$ and $\gamma = -e^T Du$. We also obtain an expression for u in terms of A and D as

$$u = \left(\frac{I}{\nu} + HH^T\right)^{-1} e,$$

where $H = D[A \ -e]$.

Another expression of u could also be derived by applying the Sherman-Morrison-Woodbury formula:

$$u = \nu\left[I - H\left(\frac{I}{\nu} + H^T H\right)^{-1} H^T\right] e.$$

Comparing the two expressions, the latter one involves the inversion of a much smaller dimensional matrix of order $(n+1)\times(n+1)$. Having solved for w and γ, given a point x, we classify x by

$$x^T w - \gamma \begin{cases} > 0, \text{ then } x \in A+, \\ < 0, \text{ then } x \in A-, \\ = 0, \text{ then } x \in A+ \text{ or } x \in A-. \end{cases}$$

2.1.2 A different expression

We found an additional derivation which gives an equivalent way of solving the minimization problem. From the same constraint in Equation (1), we have the expression for y which is $y = e - D(Aw - e\gamma)$. To minimize $f(w,\gamma,y)$, we substitute y in terms of D, A and γ into the equation which then becomes

$$\begin{aligned} f(w,\gamma,y) &= \frac{\nu}{2}\left[e - D(Aw - e\gamma)\right]^T\left[e - D(Aw - e\gamma)\right] + \frac{1}{2}(w^T w) + \frac{1}{2}\gamma^2 \\ &= \frac{\nu}{2}\left[e^T - (w^T A^T - \gamma e^T)D^T\right]\left[e - D(Aw - e\gamma)\right] + \frac{1}{2}(w^T w) + \frac{1}{2}\gamma^2 \\ &= \frac{\nu}{2}\left[e^T e - 2e^T D(Aw - e\gamma) + (w^T A^T - \gamma e^T)D^T D(Aw - e\gamma)\right] + \frac{1}{2}w^T w + \frac{1}{2}\gamma^2 \\ &= \frac{\nu}{2}\left[e^T e - 2e^T DAw + 2e^T De\gamma + w^T A^T Aw - 2\gamma e^T Aw + \gamma e^T e\gamma\right] + \frac{1}{2}w^T w + \frac{1}{2}\gamma^2 \\ &= \frac{\nu}{2}e^T e - \nu e^T DAw + \nu e^T De\gamma + \frac{\nu}{2}(w^T A^T Aw) - \nu\gamma e^T Aw + \frac{\nu}{2}\gamma^2 N + \frac{1}{2}w^T w + \frac{1}{2}\gamma^2 \end{aligned}$$

where N is the number of rows in vector e. To solve for w and γ, we set the derivatives of $f(w,\gamma,y)$ with respect to w and γ to zero:

$$\begin{cases} \dfrac{\partial f(w,\gamma,y)}{\partial w} = -\nu A^T D^T e + \nu A^T Aw - \nu A^T e\gamma + w = 0, \\ \dfrac{\partial f(w,\gamma,y)}{\partial \gamma} = \nu e^T De - \nu e^T Aw + \nu N\gamma + \gamma = 0. \end{cases} \tag{3}$$

From Equation (3), we then obtain

$$\gamma = \frac{\nu e^T Aw - \nu e^T De}{1 + \nu N}, \tag{4}$$

and substitute γ using Equation (4) in the first part of Equation (3) to obtain

$$\nu A^T Aw + w - \nu \left(A^T D^T e + A^T e \frac{\nu e^T Aw - \nu e^T De}{1 + \nu N} \right) = 0$$

$$\nu A^T Aw + w - \frac{\nu^2 A^T e e^T A}{1 + \nu N} w - \nu A^T D^T e + \frac{\nu^2 A^T e e^T De}{1 + \nu N} = 0$$

$$\left(\nu A^T A + I - \frac{\nu^2 A^T JA}{1 + \nu N} \right) w = \nu A^T D^T e - \frac{\nu^2 A^T JDe}{1 + \nu N}$$

$$w = \left(\nu A^T A + I - \frac{\nu^2 A^T JA}{1 + \nu N} \right)^{-1} \left[\nu A^T D^T e - \frac{\nu^2 A^T JDe}{1 + \nu N} \right]. \tag{5}$$

Equations (4) and (5) are derived directly from Equation (1).

2.2 Weighted proximal support vector machine (WPSVM)

2.2.1 Standard method

The PSVM is shown to be sensitive to noises. To overcome the drawback, a weighted PSVM was proposed which gives a weight to each point by taking the distance between each point and the center of its corresponding class into account [3][4].

Similar to Equation (1), we take S which denotes the weight into $f(w, \gamma, y)$, then we get a new equation called $g(w, \gamma, y)$. Note that if S is the identity matrix, $f(w, \gamma, y)$ and $g(w, \gamma, y)$ are equivalent.

$$\min g(w, \gamma, y) = \min_{w,\gamma,y} \left[\frac{\nu}{2} \|Sy\|^2 + \frac{1}{2}(w^T w) + \frac{1}{2}\gamma^2 \right] \tag{6}$$

$$\text{s.t } D(Aw - e\gamma) + y = e.$$

Let $z = Sy$, $e_1 = Se$, $A_1 = SA$ and $D_1 = SDS^{-1}$, then

$$\begin{aligned} z &= -SD(Aw - e\gamma) + Se \\ &= -SDS^{-1}(SAw - Se\gamma) + Se \\ &= -SDS^{-1}(A_1 w - e_1\gamma) + e_1 \\ &= -D_1(A_1 w - e_1\gamma) + e_1. \end{aligned}$$

Following similar steps of deriving w and γ shown in the section 2.1, we obtain the following equations for w and γ,

$$\gamma = \frac{\nu e^T S^2 Aw - \nu e^T S^2 De}{1 + \nu N} \tag{7}$$

$$w = \left(\nu A^T S^2 A + I - \frac{\nu^2 A^T S^2 J S^2 A}{1 + \nu N} \right)^{-1} \left(\nu A^T S^2 D^T e - \frac{\nu^2 e^T S^2 De A^T S^2 e}{1 + \nu N} \right). \tag{8}$$

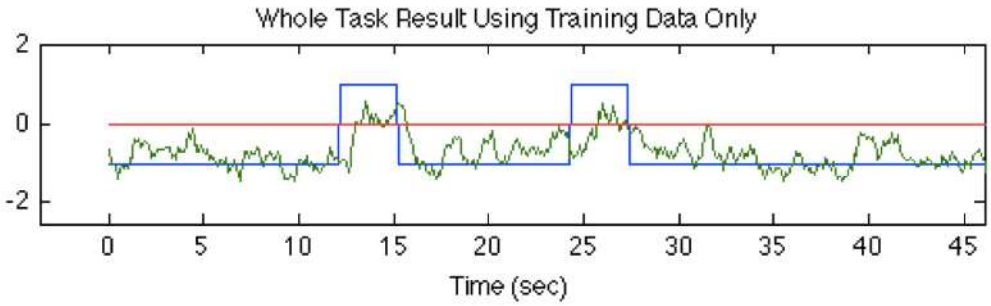

Figure 1: Classification by using the PSVM. The green line is the classifying attempt (i.e. $x^T w - \gamma$). The blue line is -1 when the cue under observation has not been cued and $+1$ when the command is cued. The red line is 0. Hence, when the green line is above the red line, we classify that data point as the action having occurred. Otherwise, we classify the data point as the action not having occurred.

2.2.2 Adapted method

Since the standard WPSVM did not improve the performance in detection rates and false positives, a new way to define the weight matrix, S, was developed. The data we analyzed had a much higher number of points in the $A-$ (or -1) classification as opposed to the $A+$ (or $+1$) classification. Hence, it is reasonable to assume that the points in the -1 classification are getting more weight in a sense. To counteract this, a new way of defining the weight of each point was developed for this specific data construction.

Suppose the y vector is permuted so that all the points for classification $+1$ correspond to the top part of the vector y, and the other points are at the bottom of y. Then y^T is defined as (y_1^T, y_2^T) where y_1 contains all of the points pertaining to classification $+1$ and y_2 is the vector containing all of the other points. Then define $||y||_w^2 = \frac{n}{n+m}||y_1||^2 + \frac{m}{n+m}||y_2||^2$, where m is the length of y_1 and n is the length of y_2.

Equivalently, if S^* is the diagonal matrix with entries $S^*_{ii} = \sqrt{n/(n+m)}$ for $1 \leq i \leq m$ and $S^*_{ii} = \sqrt{m/(n+m)}$ otherwise, then $||y||_w^2 = ||S^* y||^2$. Once obtaining S^*, we substitute S^* instead of S in Equation (7) and Equation (8) to get w and γ.

3 Data analysis with different SVM methods

3.1 Support vector machines and definition of event occurred

In section 2, we introduced and compared different support vector machine methods. In this section, we visually examine the difference between the various methods.

Figure 1 shows a small sample of the neuronal activity classified using the PSVM method. Ideally the green line would exactly match the blue line, but a common problem was the green line would seldom reach $+1$. In the original work, the red line was biased downward, which resulted in a higher rate of classification during cues, but also resulted in a higher rate of false positives.

Figure 2 shows the classification we obtained by applying the adapted WPSVM with the same data we analyzed in Figure 1. As can be seen, this classifier moves the cued data closer to the value $+1$, which remedies the problem observed in using the PSVM method.

Unfortunately, a new issue arises; occasionally a momentary spike in neural activity is found which was not cued as illustrated in Figure 3. The original algorithm for determining false positives would consider this spike as a false positive, but the spike is over a such a small time period that it should not be counted as detecting a cue. Instead, one should get a measure of the classification over a small window of time. Thus, instead of determining whether an event occurred or not by just one data point, we suggest adding the rates of all the data points within a small window. In our analysis, we used a window of one second centered around each time point to determine detection and false positive rates.

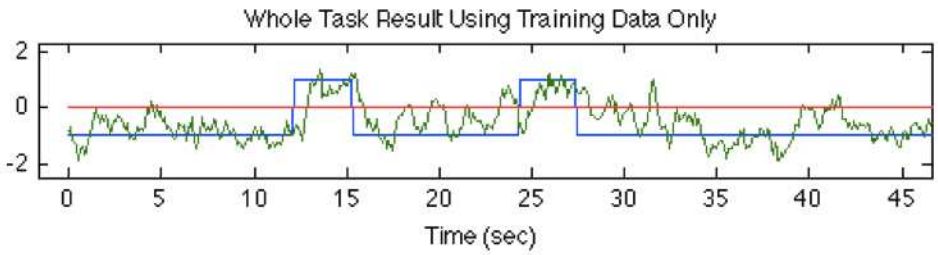

Figure 2: Classification by using the adapted WPSVM. Note that we now obtain spikes that reach a magnitude of +1 in the cued sections.

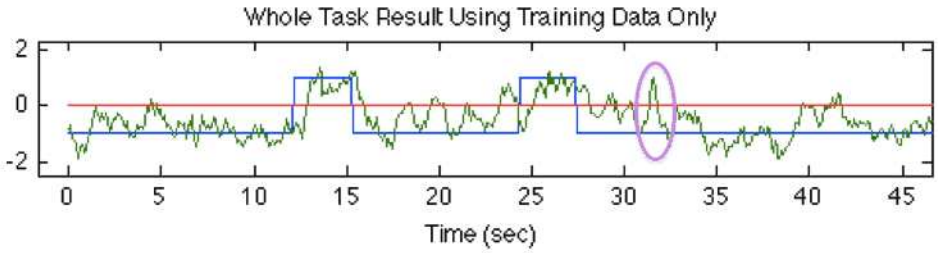

Figure 3: Classification by using the adapted WPSVM. A momentary spike in neural activity, circled in purple, is found which was not cued.

Detection Rates			
	Original PSVM	Weighted PSVM	adapted Weighted PSVM
wrist up	72.1	61.5	78.7
wrist down	26.4	17.4	61.2
wrist left	27.0	25.4	44.3
wrist right	42.6	22.1	56.6
False Positive Rates			
	Original PSVM	Weighted PSVM	adapted Weighted PSVM
wrist up	6.4	3.2	12.8
wrist down	7.1	3.0	11.7
wrist left	4.6	2.1	9.5
wrist right	10.4	7.9	18.7

Table 1: Comparison in detection and false positive rates using various PSVM and the original detection method

Detection Rates			
	Original PSVM	Weighted PSVM	adapted Weighted PSVM
wrist up	73.8	63.1	80.3
wrist down	16.5	0.8	51.2
wrist left	29.5	27.0	43.4
wrist right	38.5	5.7	55.7
False Positive Rates			
	Original PSVM	Weighted PSVM	adapted Weighted PSVM
wrist up	5.0	0.7	7.8
wrist down	3.9	0.7	8.2
wrist left	1.7	0.9	3.8
wrist right	7.8	5.0	13.5

Table 2: Comparison in detection and false positive rates using various PSVM and the one-second window detection method.

3.2 Comparison of detection and false positive rates

In Tables 1 and 2, both the original method of detection and the new method of detection are shown for all of the support vector machines (i.e., PSVM, standard WPSVM and adapted WPSVM). The tables represent a small sample of all the data analyzed.

For each patient, analyses were implemented for detection rates and false positive rates. All of the analyses are conducted at a significance level of 5% using the two-way repeated-measures ANOVA. The two factors used were (i) detection methods (with two levels) and (ii) classifiers (with three levels). All the data analyzed satisfied the assumptions of the two-way repeated-measures ANOVA. Table 3 summarizes the results.

A more detailed description of these results are as follows:

a. For SCI3, each of the three classifiers performs differently from the other two, regardless of the detection method. In addition, the adapted weight PSVM performs better (has higher detection rate) than the other two. On average, the difference between the adapted weight PSVM and the PSVM detection rate was at least 7.58% and at most 17.78%.

b. For the original detection method, all three classifiers perform differently (all p-values were < 0.0001). Furthermore, on average, the difference between the adapted weight PSVM and the PSVM in the false positive rate was at least 4.82% and at most 5.78%. For the new detection method, all three classifiers also perform differently (all p-values were < 0.0001). Additionally, on average, the difference between the adapted weight PSVM and the PSVM in the false positive rate was at least 3.73% and at most 4.69%.

	SCI3 patient			
	Detection Rates		False Positive Rates	
	significance	p-value	significance	p-value
Interaction	NO	0.152	Yes	0.0005
Detection	YES	0.0296	Yes	$< .0001$
Classifier	YES	$< .0001$	Yes	$< .0001$
	ALS patient			
	Detection Rates		False Positive Rates	
	significance	p-value	significance	p-value
Interaction	No	0.0531	No	0.3421
Detection	Yes	$< .0001$	Yes	$< .0001$
Classifier	Yes	$< .0001$	Yes	$< .0001$

Table 3: Summary of the analyses on both patients

c. For ALS, regardless of the detection method the WPSVM performs differently than the PSVM and the adapted weight PSVM, however the last two do not perform significantly differently. That is, adapted weight PSVM did not improve the detection rate from the PSVM.

d. On average, the adapted weight PSVM increases the ratio of the false positive rates from the PSVM by at most 1.43% for ALS.

4 Mapping Neuronal Activity

Of interest is the spatial distribution of neurons that significantly change activity levels during various motions. Such knowledge may lend insight to the functions for which various neurons are associated. To this end, we took the given data and constructed heat maps illustrating a measure of change in neuronal activity, as recorded by the electrodes on the implant. These maps are a visual representation of the magnitudes of the entries of a matrix. In this paper, we used warm (red) colors to denote positive values, with an increase in magnitude corresponding to darker colors, and cool (blue) colors to denote negative values.

4.1 Developing Heat Maps

In this section, we describe the development of a heat map to illustrate neuronal activity as recorded by the electrode array implant. We assumed that the number of instances a particular neuron fires over a given period of time is Poisson distributed. Furthermore, for each particular cue type (e.g., "rest", "wrist up"), we assumed the Poisson distribution describing the number of firings of a particular neuron is stationary over time.

Although this assumption allows for tractability, it may often be incorrect. The two particular neurons shown in Figure 4 illustrate an example of a relatively stationary and a non-stationary distribution of neuronal firing counts. If we take the set of counts for each neuron and compute the sample mean and variance, we can get a measure of how much our assumption of a stationary Poisson process is being violated. For each neuron, if our assumption is met, then we expect the sample mean and variance to be equal, and hence, the ratio to be near 1. Thus, we computed the ratio (mean/variance) for each neuron and then plotted these values. Figure 5 shows an example of such a plot, with neurons sorted in ascending order of the ratio values. Note that the great majority of values fell outside an arbitrarily chosen threshold, and so we have good evidence that a reproduction of this study, with non-stationary distributions taken into account will be needed to further improve the results. However, we note that a violation of our assumption merely masks smaller M.I.s; hence, in this paper, large M.I. values truly indicate significant changes in activity.

As part of constructing the heat map, we first considered the number of firings corresponding to each rest period of a task for individual neurons. Then we calculated the sample mean ($\overline{N_r}$) and variance ($\mathrm{Var}(N_r)$) of neuronal firing counts for each of the neurons associated with that particular task to obtain a summary of the baseline neuronal firing counts. Next, for each non-rest period we calculated the sample mean neuronal

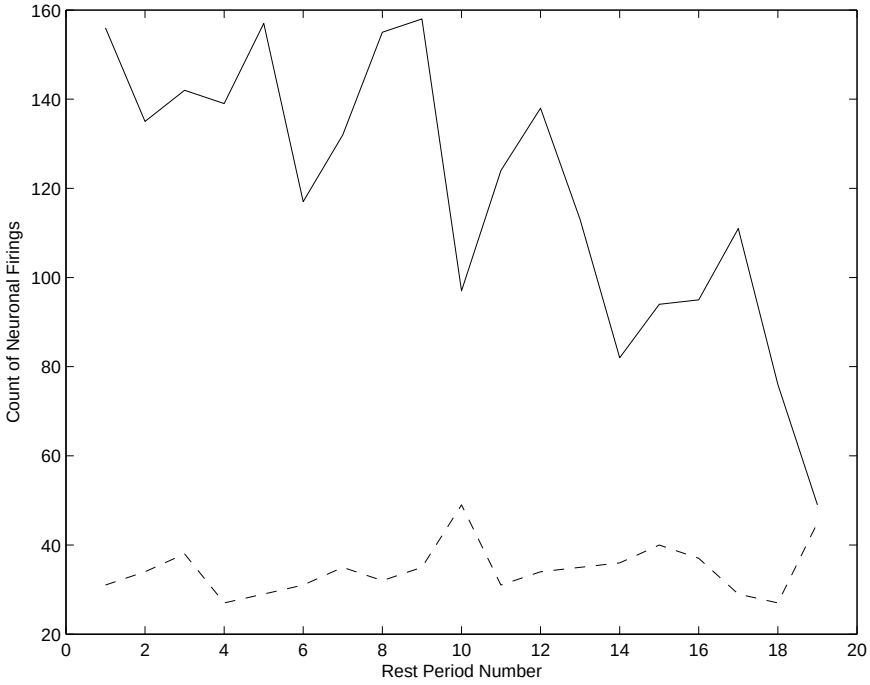

Figure 4: Neuronal firing counts for two particular neurons over the 19 different rest periods that were included in a particular example task. The dashed line shows a neuron that is stationary over time, while the solid line is one that is non-stationary over time.

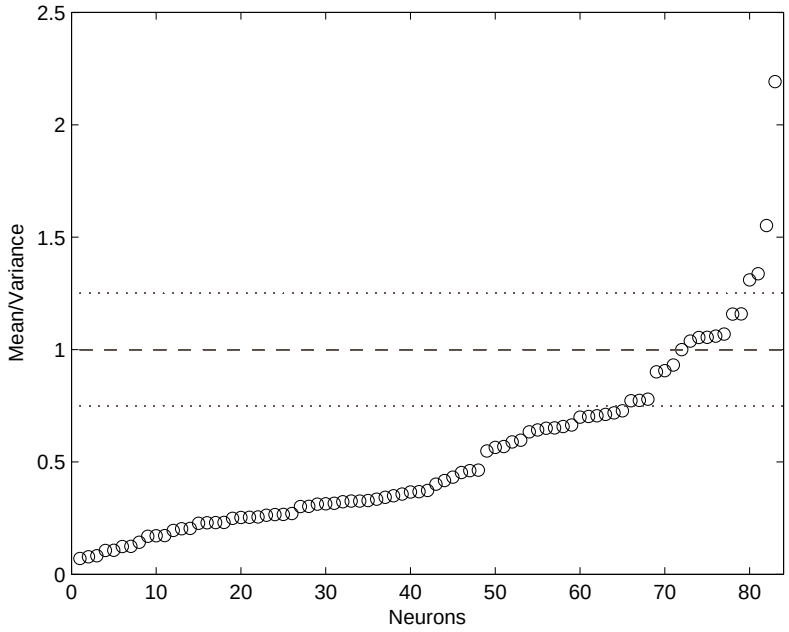

Figure 5: The ratio of mean to variance for each neuron in a particular example task, sorted into ascending order. The open circles represent the ratio for each neuron; the dashed line indicates where the ratio should be if our assumption of a stationary Poisson distribution is correct; and the dotted lines show an arbitrarily chosen threshold for which we may consider our assumption to be good enough.

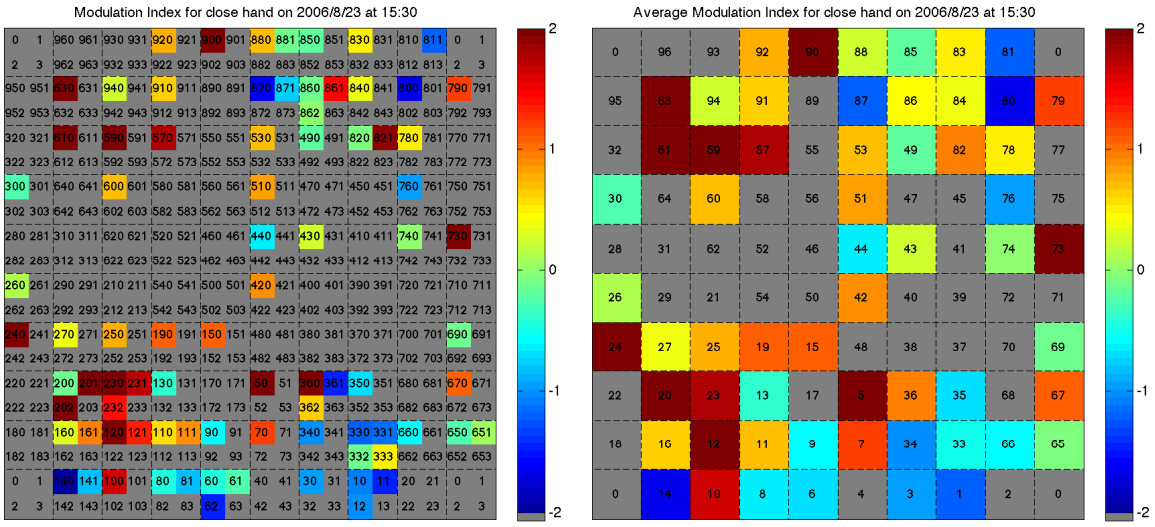

(a) (b)

Figure 6: (a) The relative neuronal activity of all individual neurons associated with the electrodes in the implant; (b) The neuronal activity associated with each electrode in the implant. These two maps show the "close hand" action of patient SCI3 on 2006/8/23 at 15:30. Note that the colors represented in a particular electrode of the condensed heat map is the average of colors represented for all neurons in the corresponding electrode of the expanded heat map. In both of these, and all other heat maps shown in this paper, we arbitrarily chose limits of -2 and 2 for the color range to give the best balance of colors displayed.

firing count ($\overline{N_m}$) related to each task, which gives the cued neuronal firing counts. Using these values we calculated the relative change in neuronal activity between the rest and non-rest periods, which is measured using a modulation index (M.I.) that we define as

$$\text{M.I.} = \frac{\overline{N_m} - \overline{N_r}}{\sqrt{\text{Var}(N_r)}}. \tag{9}$$

Using Equation (9) we calculated the M.I. for each identified neuron associated with a particular task. In the implant there can be zero to four neurons affiliated with each electrode, so to see the relative activity of each neuron we map their identifying numbers to an expanded representation of the electrode array (giving us a 20×20 matrix including the unused electrodes) and store the corresponding M.I. values. This generates the underlying matrix used to produce an expanded heat map (HM) of all the neurons associated with each electrode.

Also, instead of mapping the activity corresponding to all of the neurons, we could generate a heat map showing the activity detected by each electrode. To do this we took the sample mean value of the M.I.s of the neurons associated with each electrode and mapped them to a 10×10 matrix that represents the electrode array. From this, we generated a condensed heat map (HMC). Figure 6 illustrates the difference between a HM and a HMC. In each, the gray cells represent unused electrodes or a lack of detected neuronal activity.

4.2 Results

We generated and analysed heat maps showing the neuronal activities associated with two opposite motions, "wrist up" and "wrist down", for SCI3 during four different tasks on 2006/8/23. For each of the first three tasks, the patient was given five different cues, while in the last task she performed twelve different motions. We can do the same for other movements as well, but for the scope and purpose of this paper, we limited our analysis to this pair of motions over this specific session.

We first considered the HMCs shown in Figures 7a and 7b. As the cue given changed between "wrist down" and "wrist up", it was clear that the overall neuronal firing rate decreased. All the dark red colored

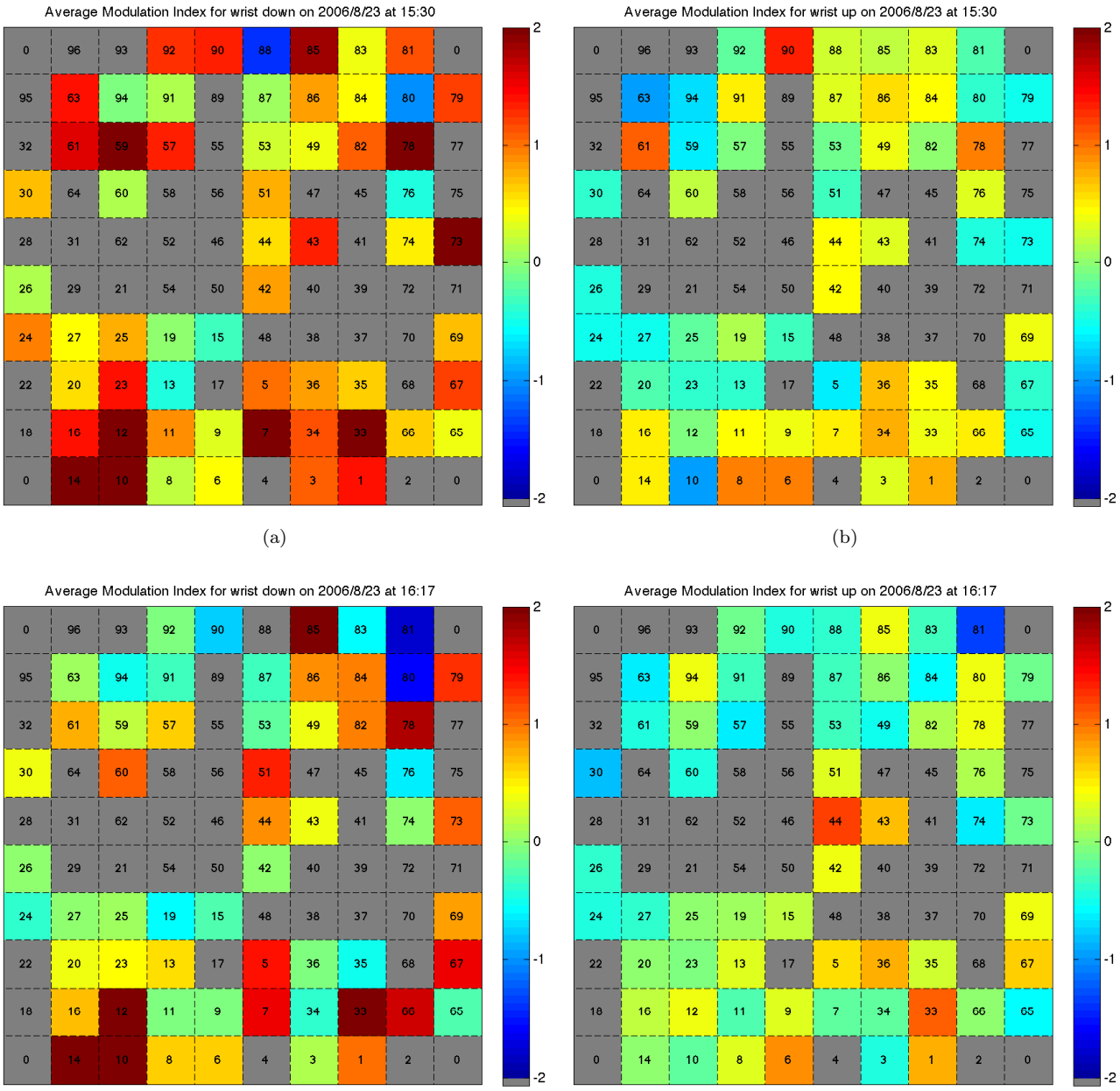

(a) (b)

(c) (d)

Figure 7: HMCs for each of the cues "wrist down" and "wrist up" for SCI3's session that took place on 2006/8/23.

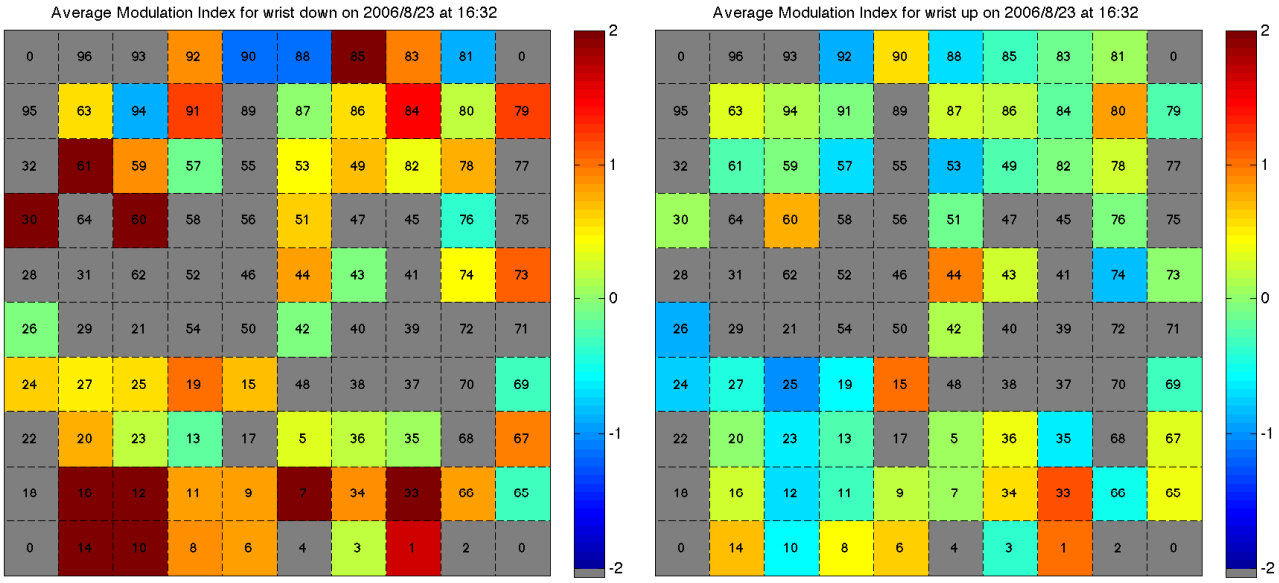

(e)

(f)

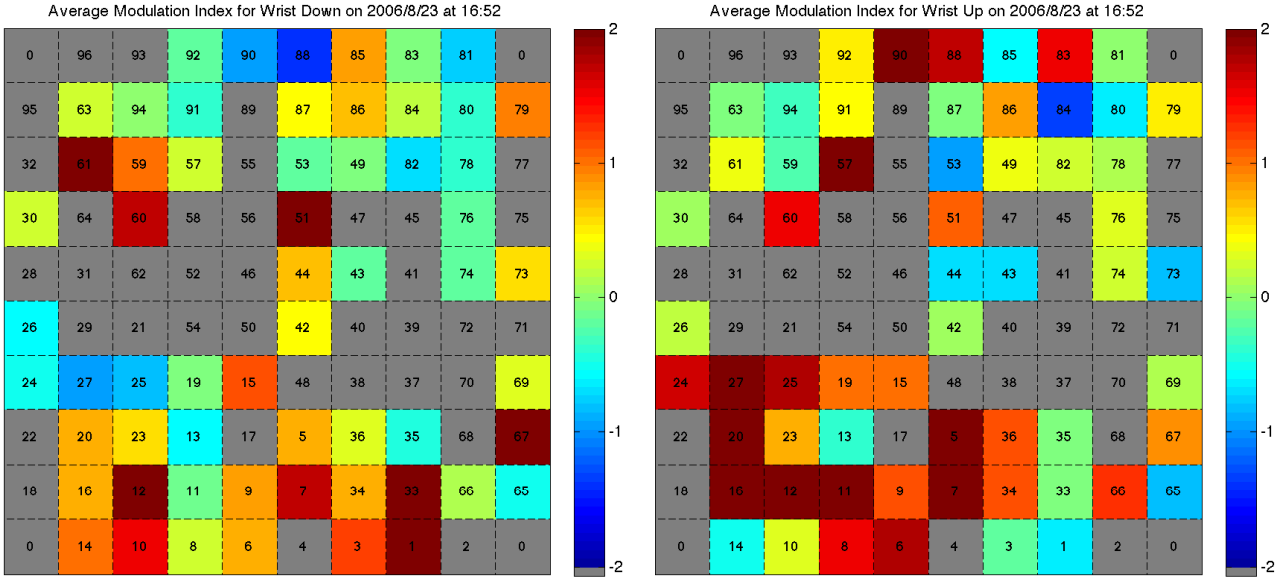

(g)

(h)

Figure 7: continued

electrodes which showed high neuronal activity during the "wrist down" movement changed to low neuronal activity during the "wrist up" movement. At the same time, firing activity increased in some electrodes, shown as a change from cool to warm shades. For example, the electrodes labeled 88, 91, 87, 80 and 76 show a clear increase in neuronal activity, although not all the increases were of the same magnitude. Also some electrodes had M.I.s near zero and did not show a color change when going from "wrist down" to "wrist up", such as the electrodes labeled 15 and 13. This may be evidence that those electrodes are not associated with either of the movements.

The same general pattern of similarities and differences observed between Figures 7a and 7b are also seen when comparing Figures 7c and 7d as well as Figures 7e and 7f. While specific electrodes identified above may change between the tasks, the qualitative conclusions are analogous.

Next, we consider the HMCs in Figures 7g and 7h. Here, we see a different pattern from that of the other heat maps. As we are going from "wrist down" to "wrist up", the neuronal firing rate increases. All the dark red colored electrodes (except number 12) which show high neuronal activity during the "wrist down" movement change to low neuronal activity during the "wrist up" movement. At the same time firing activity increased in a number of electrodes. Compared to all of the other heat maps, we see many, but not all, of the same electrodes registering an increase in activity as the subject is given the different cues; many other neurons also show increased activity. This difference may be due to the fact that in this task SCI3 was undergoing twelve different cued motions, which may have created more neuronal activity. Here only electrode 94 had a M.I. near zero and did not show a color change when going between "wrist down" and "wrist up"; this may be evidence that this electrode is not associated with either of the movements.

From this preliminary work, it is clear that the neuronal activity changes for different movements. In all the heat maps shown in Figure 7 we see that one electrode (number 13), while not near zero, did not show a color change when going from "wrist down" to "wrist up"; this may be an indication that the neurons associated with this electrode are not related to either of the movements. Also one electrode (number 88) showed an increase in neuronal firing activity during each task as the subject is going from "wrist down" to "wrist up", possibly giving evidence that those neurons are related to executing a "wrist up" motion.

5 Conclusion

In the present work, we developed various modifications to the classifiers originally used. The modifications showed mixed results of improvements. In particular, the adapted WPSVM method produced increased detection rates while also increasing false positive rates. This results in a trade off of what is most important for the application. We also developed methods for converting the data in to heat maps, which gave a visual representation of neural activity and may aid in determining the neurons that are associated with various movements of the arm.

Future work will need to reexamine the assumptions on which we based our methods, and, in particular, determine how accounting for a non-stationary distribution of neuronal firing counts over time affects the results given. Also, a more quantitative analysis of the data/heat maps may provide deeper insight in to the association between individual neurons and motor controls. Developing and utilizing different measures for recognizing significant changes in neural activity, i.e., expressions for the M.I., may likewise prove fruitful.

References

[1] Wikipedia: the free encyclopedia *Electromagnetic theories of consciousness,* <http://en.wikipedia.org/wiki/Electromagnetic_theories_of_consciousness>.

[2] Glenn Fung and Olvi L. Mangasarian, *Proximal Support Vector Machine Classifiers,* Computer Sciences Department, University of Wisconsin, 1210 West Dayton Street, Madison, WI 53706.

[3] Meng Zhang, Caofeng Wang, and Lihua Fu, *Robustness Enhancement for Proximal Support Vector Machines,* IEEE, 2004.

[4] ZHANG Meng, FU Li-hua, WANG Gao-feng, and HU Ji-cheng, *Weighted Proximal Support Vector Machines: Robust Classification,* Wuhan University Journal of Natural Science, Vol. 10, No. 3, 2005.